Mon. Not. R. Astron. Soc. **000**, 1–7 (2011) Printed 13 November 2012 (MN LATEX style file v2.2)

The intrinsic shapes of prestellar cores

O. Lomax⋆, A. P. Whitworth and A. Cartwright
School of Physics and Astronomy, Cardiff University, Cardiff CF24 3AA

13 November 2012

ABSTRACT

Using observations of prestellar cores to infer their intrinsic properties requires the solution of several poorly constrained inverse problems. Here we address one of these problems, namely to deduce from the observed aspect ratios of prestellar cores their intrinsic three-dimensional shapes. Four models are proposed, all based on the standard assumption that prestellar cores are ellipsoidal, and on the further assumption that a core's shape is not correlated with its absolute size. The first and simplest model, **M1**, has a single free parameter, and assumes that the relative axes of a prestellar core are drawn randomly from a log-normal distribution with zero mean and standard deviation $\tau_{\rm o}$. The second model, **M2a**, has two free parameters, and assumes that the log-normal distribution (with standard deviation $\tau_{\rm o}$) has a finite mean, $\nu_{\rm o}$, defined so that $\nu_{\rm o} < 0$ means elongated (or filamentary) cores are favoured, whereas $\nu_{\rm o} > 0$ means flattened (or disc-like) cores are favoured. Details of the third model (**M2b**, two free parameters) and the fourth model (**M4**, four free parameters) are given in the text. Markov chain Monte Carlo sampling and Bayesian analysis are used to map out the posterior probability density functions of the model paramaters, and the relative merits of the models are compared using Bayes factors. We show that **M1** provides an acceptable fit to the data with $\tau_{\rm o} \approx 0.57 \pm 0.06$; and that, although the other models sometimes provide an improved fit, there is no strong justification for the introduction of their additional parameters.

Key words: methods: statistical – stars: formation – ISM: clouds – submillimetre: ISM

1 INTRODUCTION

There have been several previous models developed to fit the observed aspect ratios of cores, using both randomly oriented spheroids (e.g. Myers et al. 1991; Ryden 1996) and randomly oriented ellipsoids (e.g. Goodwin et al. 2002; Jones & Basu 2002; Tassis 2007). These models invoke from two to four free parameters. In this paper we introduce a model in which the the intrinisic shapes of prestellar cores are characterised by just one free parameter. Using Markov Chain Monte Carlo sampling (MCMC), we generate a probability density function (PDF) for this parameter, based on continuum observations of the cores in Ophiuchus by Simpson et al. (2008) (SNW-T08), Stanke et al. (2006) (SSGK06) and Motte et al. (1998) (MAN98). We also define three more complex models, which, by introducing additional parameters, are better able to fit the observed distribution of projected shapes. By means of Bayesian analysis we show that these more complex models are not justified.

In Section 2 we introduce each of the models, and explain how we derive projected shapes. In Section 3 we describe how we use Bayesian analysis to identify the best-fit model parameters, and the best models, using the observational data. In Section 4 we present and discuss the results, and in Section 5 we summarize our conclusions.

1.1 Observational data

We use data from three diffent surveys of dust continuum emission. The SNW-T08 data were obtained using SCUBA on the JCMT at 850 μm; 52 cores were identified, and fitted with ellipses at the 3σ noise contour. The SSGK06 data were obtained using SIMBA on the SEST telescope at 1.2 mm; 143 cores were extracted using *Gaussclumps* (Stutzki & Güsten 1990). The MAN98 data were obtained using the MPIfR array on the IRAM telescope at 1.3 mm; 35 cores were extracted, again using *Gaussclumps*.

2 MODELLING THE SHAPES OF CORES

We follow the convention that, to a first approximation, the projected shape of a core can be approximated by an ellipse (with axes $a, b,\ \ a > b$, and aspect ration $q = b/a$); and its

⋆ E-mail: oliver.lomax@astro.cf.ac.uk

intrinsic shape by an ellipsoid (with principal axes A, B, C, $A>B>C$). In addition, we assume that the proportions of a core ($A{:}B{:}C$) are independent of its absolute size.

2.1 Model M1, one free parameter ($\tau_{\rm O}$)

The first model, **M1**, has only one free parameter, $\tau_{\rm O}$. The principal axes of a sample ellipsoid are then generated according to

$$\begin{aligned} A &= 1\,, \\ B &= \exp(\tau_{\rm O}\mathcal{G}_{\rm B})\,, \\ C &= \exp(\tau_{\rm O}\mathcal{G}_{\rm C})\,. \end{aligned} \tag{2.1}$$

Here – and in the sequel – $\mathcal{G}_{\rm B}$ and $\mathcal{G}_{\rm C}$ are random deviates drawn from a Gaussian distribution with zero mean and unit standard deviation. Increasing $\tau_{\rm O}$ increases the likelihood that the axes of a core have very disparate sizes, and hence the likelihood that the projected shape of the core has a small aspect ratio, q.

2.2 Model M2a, two free parameters ($\nu_{\rm O}, \tau_{\rm O}$)

The second model, **M2a**, has two free parameters, $\nu_{\rm O}$ and $\tau_{\rm O}$. The principal axes of a sample ellipsoid are then generated according to

$$\begin{aligned} A &= 1\,, \\ B &= \exp(\nu_{\rm O} + \tau_{\rm O}\mathcal{G}_{\rm B})\,, \\ C &= \exp(\nu_{\rm O} + \tau_{\rm O}\mathcal{G}_{\rm C})\,. \end{aligned} \tag{2.2}$$

If $\nu_{\rm O} > 0$, the cores have a tendency to be disc-like; with $\tau_{\rm O} = 0$, they are oblate spheroids. If $\nu_{\rm O} < 0$, the cores have a tendency to be filamentary; with $\tau_{\rm O} = 0$, they are prolate spheroids.

2.3 Model M2b, two free parameters ($\tau_{\rm B}, \tau_{\rm C}$)

The third model, **M2b**, has two free parameters, $\tau_{\rm B}$ and $\tau_{\rm C}$. The principal axes of a sample ellipsoid are then generated according to

$$\begin{aligned} A &= 1\,, \\ B &= \exp(\tau_{\rm B}\mathcal{G}_{\rm B})\,, \\ C &= \exp(\tau_{\rm C}\mathcal{G}_{\rm C})\,. \end{aligned} \tag{2.3}$$

2.4 Model M4, four free parameters ($\nu_{\rm B}, \tau_{\rm B}, \nu_{\rm C}, \tau_{\rm C}$)

The fourth model, **M4**, has four free parameters, ($\nu_{\rm B}$, $\tau_{\rm B}$, $\nu_{\rm C}$ and $\tau_{\rm C}$. The principal axes of a sample ellipsoid are then generated according to

$$\begin{aligned} A &= 1\,, \\ B &= \exp(\nu_{\rm B} + \tau_{\rm B}\mathcal{G}_{\rm B})\,, \\ C &= \exp(\nu_{\rm C} + \tau_{\rm C}\mathcal{G}_{\rm C})\,. \end{aligned} \tag{2.4}$$

2.5 Projecting an arbitraily oriented ellipsoid

Once the principal axes of a core have been generated, they are re-ordered so that $A>B>C$. Next, without loss of generality, we define a Cartesian co-ordinate system in which the x-axis is aligned along A, the y-axis along B, and the z-axis along C. To observe this core from an arbitrary direction, given by polar angles (θ, ϕ), we set

$$\theta = \cos^{-1}(2\mathcal{R}_\theta - 1)\,, \tag{2.5}$$

$$\phi = 2\pi\mathcal{R}_\phi\,, \tag{2.6}$$

where $\mathcal{R}_\theta$ and $\mathcal{R}_\phi$ are random deviates from a uniform distribution on the interval $(0, 1)$. The aspect ratio of the core is then given by

$$q = \sqrt{\frac{\alpha+\gamma-\sqrt{(\alpha-\gamma)^2+\beta^2}}{\alpha+\gamma+\sqrt{(\alpha-\gamma)^2+\beta^2}}} \tag{2.7}$$

where

$$\alpha = (A^2\cos^2(\phi) + B^2\sin^2(\phi))\cos^2(\theta) + C^2\sin^2(\theta), \tag{2.8}$$

$$\beta = (B^2 - A^2)\cos(\theta)\sin(2\phi), \tag{2.9}$$

$$\gamma = A^2\sin^2(\phi) + B^2\cos^2(\phi) \tag{2.10}$$

(see Binney 1985).

3 BAYESIAN ANALYSIS

We use Bayesian analysis to determine the best-fit parameters of the different models, and to quantify their relative strengths. When comparing model $\mathbf{M}$ with parameters $\mathbf{x} \equiv (x_1, x_2, ...)$ against observational data $\mathbf{D}$, Bayes' theorem states that

$$P(\mathbf{x}|\mathbf{M},\mathbf{D}) = \frac{P(\mathbf{D}|\mathbf{M},\mathbf{x})P(\mathbf{x}|\mathbf{M})}{P(\mathbf{D}|\mathbf{M})}\,. \tag{3.1}$$

Here $P(\mathbf{x}|\mathbf{M},\mathbf{D})$ is the posterior probability of $\mathbf{x}$ given $\mathbf{D}$, $P(\mathbf{D}|\mathbf{M},\mathbf{x})$ is the likelihood of $\mathbf{D}$ given $\mathbf{x}$, $P(\mathbf{x}|\mathbf{M})$ is the prior PDF of $\mathbf{x}$ and $P(\mathbf{D}|\mathbf{M})$ is the marginal likelihood over all values of $\mathbf{x}$, i.e.

$$P(\mathbf{D}|\mathbf{M}) = \int_{\mathbf{x}} \mathbf{P}(\mathbf{D}|\mathbf{M},\mathbf{x})\mathbf{P}(\mathbf{x}|\mathbf{M})\,{\rm d}\mathbf{x}\,. \tag{3.2}$$

As $P(\mathbf{D}|\mathbf{M})$ is a constant, equation (3.1) simplifies to

$$P(\mathbf{x}|\mathbf{M},\mathbf{D}) \propto \mathbf{P}(\mathbf{D}|\mathbf{M},\mathbf{x})\mathbf{P}(\mathbf{x}|\mathbf{M})\,, \tag{3.3}$$

where any generated posterior PDFs can be normalized to unity, post analysis.

3.1 Prior PDF

When generating prior PDFs for the model parameters $\mathbf{x}$ we assume that $P(\mathbf{x}|\mathbf{M})$ is finite and uniform within given limits, and zero outside them. This is to say, within credible limits, we impose no *a priori* preference for any specific $\mathbf{x}$.

For **M1**, the single parameter $\tau_{\rm O}$ must be able to reproduce the maximum and minimum observed aspect ratios in the data, viz. $q_{\rm MAX} \simeq 1$ and $q_{\rm MIN} \simeq 0.3$ (over all three data sets, there are only two cores with $q<0.3$). Since the majority of aspect ratios delivered by **M1** satisfy $q \gtrsim \exp(-\tau_{\rm O})$, we set $-\ln(q_{\rm MAX}) \leq \tau_{\rm O} \leq -\ln(q_{\rm MIN})$, i.e. $0 \leq \tau_{\rm O} \leq 1.2$.

For **M2a** we set the range of $\nu_{\rm O}$ to $-1.2 \leq \nu_{\rm O} \leq 1.2$ so that a purely oblate or prolate population (i.e. one with $\tau_{\rm O}=0$) could reproduce the observed aspect ratios. We then assign $\tau_{\rm O}$ the same range as in **M1**.

For both **M2b** and **M4** we assign $\tau_{\rm B}$ and $\tau_{\rm C}$ the same range as $\tau_{\rm O}$ in **M1**. For **M4** we assign $\nu_{\rm B}$ and $\nu_{\rm C}$ the same range as $\nu_{\rm O}$ in **M2a**.

With these ranges, the normalised prior PDFs are:

$$P(\tau_{\rm O}|\mathbf{M1}) = \begin{cases} \frac{1}{(1.2)} & \text{if } 0 \le \tau_{\rm O} \le 1.2, \\ 0 & \text{otherwise;} \end{cases}$$

$$P(\nu_{\rm O}, \tau_{\rm O}|\mathbf{M2a}) = \begin{cases} \frac{1}{2(1.2)^2} & \text{if } -1.2 \le \nu_{\rm O} \le 1.2 \\ & \text{and } 0 \le \tau_{\rm O} \le 1.2, \\ 0 & \text{otherwise;} \end{cases}$$

$$P(\tau_{\rm B}, \tau_{\rm C}|\mathbf{M2b}) = \begin{cases} \frac{1}{(1.2)^2} & \text{if } 0 \le \tau_{\rm B} \le 1.2 \\ & \text{and } 0 \le \tau_{\rm C} \le 1.2, \\ 0 & \text{otherwise;} \end{cases}$$

$$P(\nu_{\rm B}, \nu_{\rm C}, \tau_{\rm B}, \tau_{\rm C}|\mathbf{M_4}) = \begin{cases} \frac{1}{4(1.2)^4} & \text{if } -1.2 \le \nu_{\rm B} \le 1.2 \\ & \text{and } -1.2 \le \nu_{\rm C} \le 1.2 \\ & \text{and } 0 \le \tau_{\rm B} \le 1.2 \\ & \text{and } 0 \le \tau_{\rm C} \le 1.2, \\ 0 & \text{otherwise}\,. \end{cases} \tag{3.4}$$

3.2 Markov chain Monte Carlo sampling

For each observational data set, $\mathbf{D}$, we generate a histogram of aspect ratios. The histogram has ten bins ($k = 1$ to 10), evenly spaced between $q = 0$ and $q = 1$, and O_k is the number of observed cores in bin k.

For a given model, $\mathbf{M}$, and a given choice of the associated free parameters, $\mathbf{x_i}$, we generate 10^4 ellipsoids, and view each one from an arbitrary direction to determine its aspect ratio, q, as described in Section 2. The resulting q-values are then used to construct an equivalent histogram of expectation values, E_j, ($j = 1$ to 10), normalised so that $\sum_j\{E_j\} = \sum_j\{O_j\}$. The likelihood of the observational data, $\mathbf{D}$, being reproduced by $\mathbf{M}, \mathbf{x_i}$ is then

$$P(\mathbf{D}|\mathbf{M}, \mathbf{x_i}) = \exp\left\{ - \sum_{j=1}^{j=10} \frac{(O_j - E_j)^2}{2O_j} \right\} . \tag{3.5}$$

We have assumed purely Poisson errors on the counts in each bin, because error estimates for individual q-values are not available. Bins that have less than five counts are pooled together so that the Gaussian approximation to Poisson errors is valid.

To build a Markov Chain, we consider the observational values, O_k, from a particular data set, $\mathbf{D}$, and we invoke a particular model, $\mathbf{M}$. We pick a set of model parameters ($\mathbf{x_0}$) in the middle of the ranges defined in Section 3.1, and compute $P(\mathbf{D}|\mathbf{M}, \mathbf{x_0})$, as described in the preceding paragraph. We then build the chain by stepping from one set of model parameters to another, $\mathbf{x_0} \rightarrow \mathbf{x_1} \rightarrow \mathbf{x_2} \rightarrow \mathbf{x_3}$.... Each step, $\Delta\mathbf{x} = \mathbf{x_{i+1}} - \mathbf{x_i}$ is drawn randomly from a Gaussian distribution centred on zero. The step is only made if

$$\frac{P(\mathbf{D}|\mathbf{M}, \mathbf{x_{i+1}})}{P(\mathbf{D}|\mathbf{M}, \mathbf{x_i})} \ge \mathcal{R}_{\rm STEP}\,, \tag{3.6}$$

where $\mathcal{R}_{\rm STEP}$ is a random deviate from a uniform distribution on the interval (0,1). Otherwise the step is rejected and a new step is drawn; this ensures that the points on the chain tend to concentrate in regions of high probability. The coefficients regulating the mean step size should be adjusted so that roughly half the steps are rejected. The first 10^3 points on the chain are discarded, to remove any memory of the starting point. The subsequent 5×10^5 points are used to identify the best-fit parameters and their uncertainties.

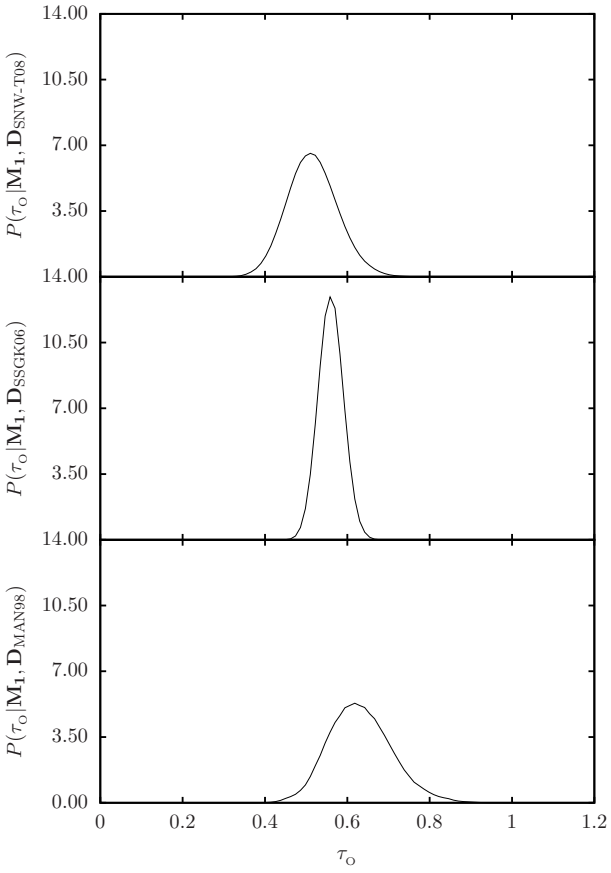

Figure 1. Posterior PDFs for $\tau_{\rm O}$ in **M1**, from the SNW-T08, SSGK06 and MAN98 data.

We have built a Markov Chain for each possible combination of the four models and the three data sets. The points on the chain are then used to determine the posterior PDFs of the model parameters. The results are presented in Figs. 1, 2, 3 and 4. The best fits obtained with **M1** and **M2a** are compared with the observations in Figs. 5 and 6.

3.3 Model selection

Bayesian analysis can also be used to compare different models. Given a list of competing models, $\mathbf{M_1}, \mathbf{M_2}, \ldots, \mathbf{M_n}$, the probability of a particular model, $\mathbf{M_k}$, is

$$P(\mathbf{M_k}|\mathbf{D}) = \frac{\mathbf{P(D}|\mathbf{M_k)P(M_k)}}{\mathbf{P(D)}}\,, \tag{3.7}$$

where

$$P(\mathbf{D}) = \sum_{\mathbf{k=1}}^{\mathbf{k=n}} \mathbf{P(D}|\mathbf{M_k)P(M_k)}\,. \tag{3.8}$$

To calculate $P(\mathbf{D}|\mathbf{M_k})$ we must marginalise each model's likelihood over its associated parameter space (see Eqn. 3.2). We evaluate this integral by organising the points on the associated Markov Chain into a balanced binary tree (Weinberg 2009). This has the effect of dividing the parameter space into cells, each of which contains a single point. Each

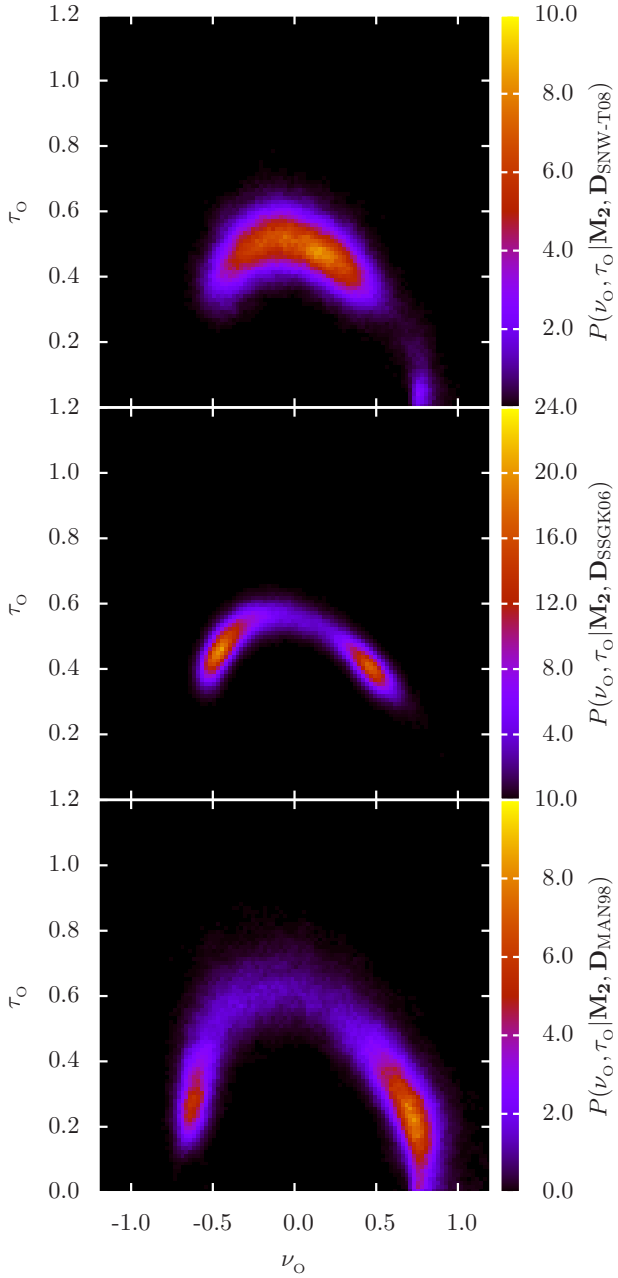

Figure 2. Posterior PDFs for $\nu_{\rm O}$ and $\tau_{\rm O}$ in **M2a**, from the SNW-T08, SSGK06 and MAN98 data.

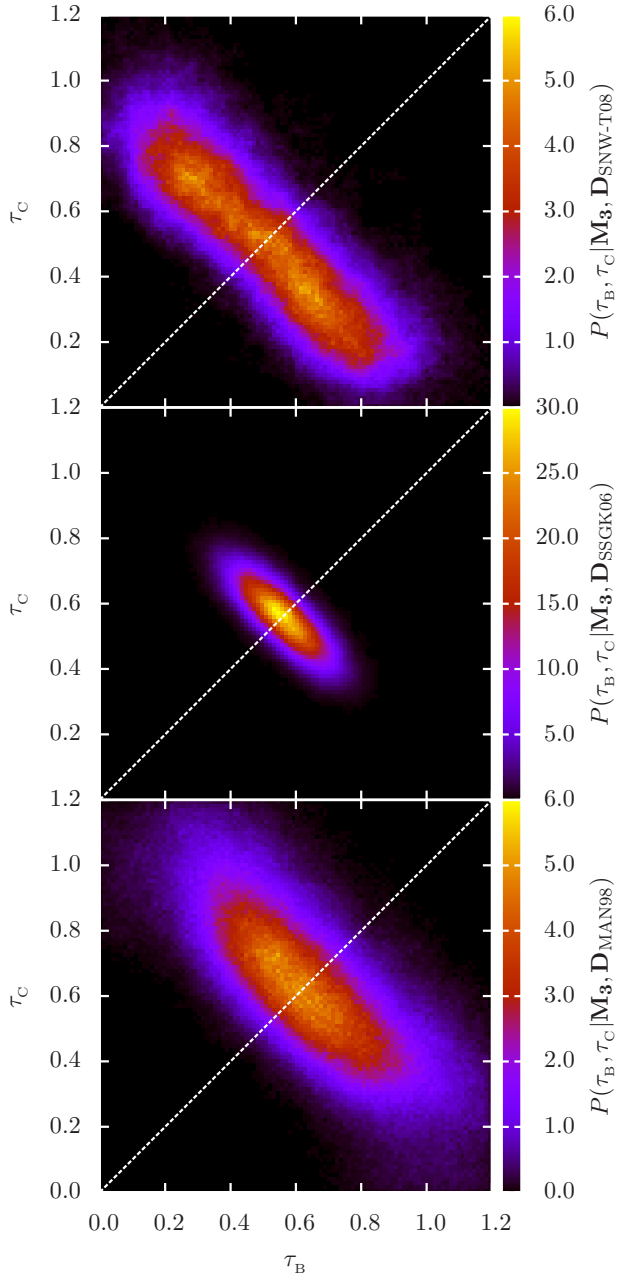

Figure 3. Posterior PDFs for $\tau_{\rm B}$ and $\tau_{\rm C}$ in **M2b**, from the SNW-T08, SSGK06 and MAN98 data. The white dashed line represents $\tau_{\rm B} = \tau_{\rm C}$, about which the distribution should be symmetric.

point, $\mathbf{x_i}$, now has a likelihood (see Eqn. 3.5) and a volume of parameter space, $\delta V_{\mathbf{i}}$ equal to the volume of the cell it occupies. Hence the marginalised likelihood is approximated by

$$P(\mathbf{D}|\mathbf{M_k}) \simeq \frac{1}{V} \sum_{\mathbf{i}=1}^{\mathbf{i}=N} P(\mathbf{D}|\mathbf{M_k}, \mathbf{x_i})\, \delta V_{\mathbf{i}}\,. \qquad (3.9)$$

Here N is the number of points on the Markov Chain and V is the total volume of parameter space associated with model $\mathbf{M_k}$. As MCMC sampling is most noisy around the edges of the distribution, we omit from the summation any cells that extend to the boundaries of the parameter space. These regions are undersampled and have disproportionately large cells; including them generally overestimates $P(\mathbf{D}|\mathbf{M_k})$.

The relative likelihood of one model, $\mathbf{k}$, with respect to another, $\mathbf{k'}$, is quantified by the Bayes factor

$$K_{\mathbf{kk'}} = \frac{P(\mathbf{M_k}|\mathbf{D})}{P(\mathbf{M_{k'}}|\mathbf{D})} = \frac{P(\mathbf{D}|\mathbf{M_k})\mathbf{P}(\mathbf{M_k})}{P(\mathbf{D}|\mathbf{M_{k'}})\mathbf{P}(\mathbf{M_{k'}})}\,. \qquad (3.10)$$

Given that we have no *a priori* preference for either model,

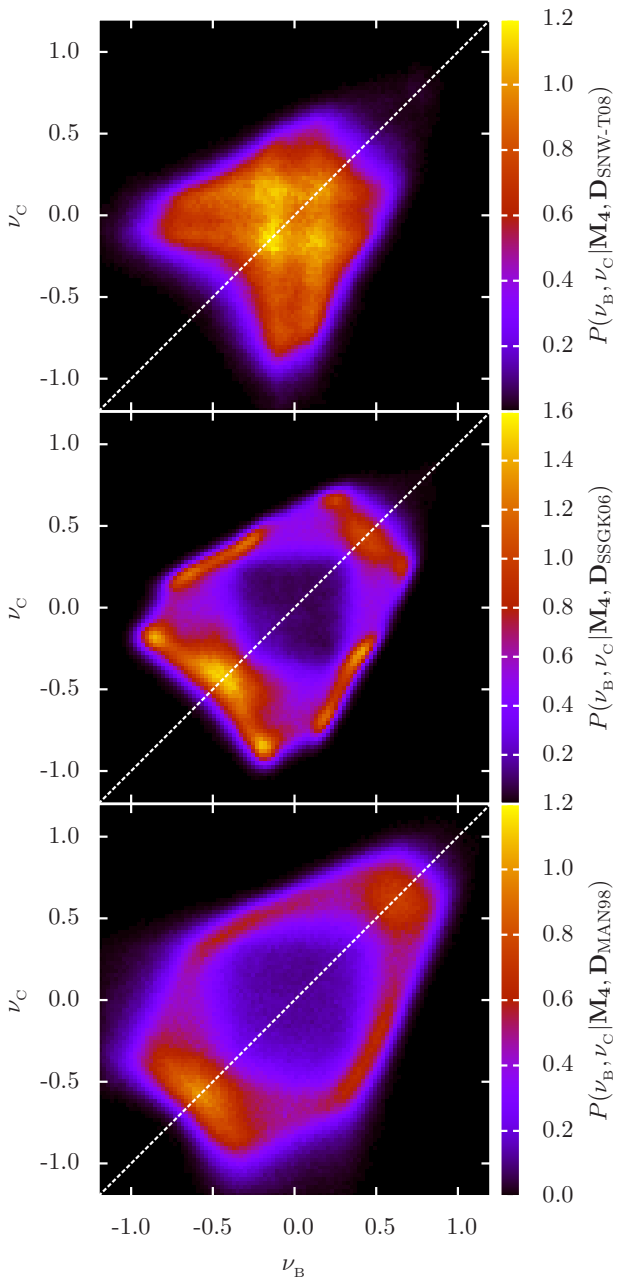

Figure 4. Posterior PDFs for $\nu_{\rm B}$, $\nu_{\rm C}$ in **M4**, from the SNW-T08, SSGK06 and MAN98 data. $\tau_{\rm B}$ and $\tau_{\rm C}$ have been marginalized out, i.e. $P(\nu_{\rm B}, \nu_{\rm C}|\mathbf{M4}, \mathbf{D}) = \iint P(\nu_{\rm B}, \nu_{\rm C}, \tau_{\rm B}, \tau_{\rm C}|\mathbf{M4}, \mathbf{D})\, {\rm d}\tau_{\rm B}\, {\rm d}\tau_{\rm C}$. The white dashed line represents $\nu_{\rm B} = \nu_{\rm C}$, about which the distribution should be symmetric.

i.e. $P(\mathbf{M_k}) = P(\mathbf{M_{k'}})$, equation (3.10) reduces to the ratio of the marginalised likelihoods. Bayes factors quantifying the relative performance of the different models are presented in Table 1 .

4 RESULTS

4.1 Parameter estimation for M1

Fig. 1 shows the posterior PDFs for $\tau_{\rm O}$ in **M1**, based on the different data sets. Since the PDFs are all unimodal and not overly skewed, we can calculate means and standard deviations, viz. $\tau_{\rm O} = 0.51 \pm 0.06\,({\rm SNW-T09})$, $0.56 \pm 0.03\,({\rm SSGK06})$, $0.63 \pm 0.08\,({\rm MAN98})$. These values can be combined to give $\tau_{\rm O} = 0.57 \pm 0.07$, i.e. the principal axes of a core typically differ by a factor of order $\exp(\tau_{\rm O}) \simeq 1.7$.

Figure 5 compares the observed distributions of aspect ratio from the different data sets with the best fits from **M1**. **M1** fits the SSGK06 data (which, with 142 cores, has the least noisy statistics) well. The fits to the SNW-T09 data (52 cores) and the MAN98 data (35 cores) are less good. For example, the MAN98 data hints at a sharp peak between $q = 0.5$ and $q = 0.6$ which **M1** is unable to reproduce; however, this may just be the product of small-number statistics.

4.2 Parameter estimation for M2a

Fig. 2 shows the posterior PDFs of $\nu_{\rm O}$ and $\tau_{\rm O}$ in **M2a**, based on the different data sets. We recall that $\nu_{\rm O}$ determines whether cores have a tendency to be filamentary ($\nu_{\rm O} < 0$) or disc-like ($\nu_{\rm O} > 0$). For all three data sets there is a degeneracy, because the intrinsic asymmetry of the cores is promoted both by increasing $\tau_{\rm O}$, and by increasing $|\nu_{\rm O}|$. Consequently solutions with reduced $\tau_{\rm O}$ and increased $|\nu_{\rm O}|$ have high probability. Indeed, for the SSGK06 and MAN98 data sets these are actually the prefered solutions. However, in neither case is there a clear preference for filamentary over disc-like cores, or *vice versa*.

Figure 6 compares the observed distributions of aspect ratio with the best fits from **M2a**. **M2a** delivers a markedly better fit – than **M1** – to the SSGK06 and MAN98 data sets, irrespective of whether we use the filamentary or disc-like parameters. However, the best fit to the SNW-T09 data set is not much better than with **M1**.

4.3 Parameter estimation for M2b

Figure 3 shows the posterior PDFs of $\tau_{\rm B}$ and $\tau_{\rm C}$ in **M2b**, based on the different data sets. For the SSGK06 data we find a peak at $\tau_{\rm B} \simeq \tau_{\rm C} \simeq 0.55$, and for the MAN98 data at $\tau_{\rm B} \simeq \tau_{\rm C} \simeq 0.60$. For the SNW-T09 data, the distribution of $\tau_{\rm B}$ and $\tau_{\rm C}$ is somewhat broader, but nowhere does it exceed that for $\tau_{\rm B} \simeq \tau_{\rm C} \simeq 0.50$. Thus, for all three data sets, the two parameters of **M2b** do not furnish a better fit than the single parameter of **M1**.

4.4 Parameter estimation for M4

Figure 4 shows the posterior PDFs of $\nu_{\rm B}$ and $\nu_{\rm C}$ in **M4**, based on the different data sets; for simplicity, we have marginalized $\tau_{\rm B}$ and $\tau_{\rm C}$ out of the PDFs. For all three data sets, the highest probabilities lie on the line $\nu_{\rm B} \simeq \nu_{\rm C}$, which suggests that **M4** is unable to improve on **M2a**. There are also regions of moderately high probability where $\nu_{\rm B} \neq \nu_{\rm C}$, but these are outweighed by the regions where $\nu_{\rm B} \simeq \nu_{\rm C}$, and there is no hint of a preference for filamentary over disc-like shapes, or *vice versa*.

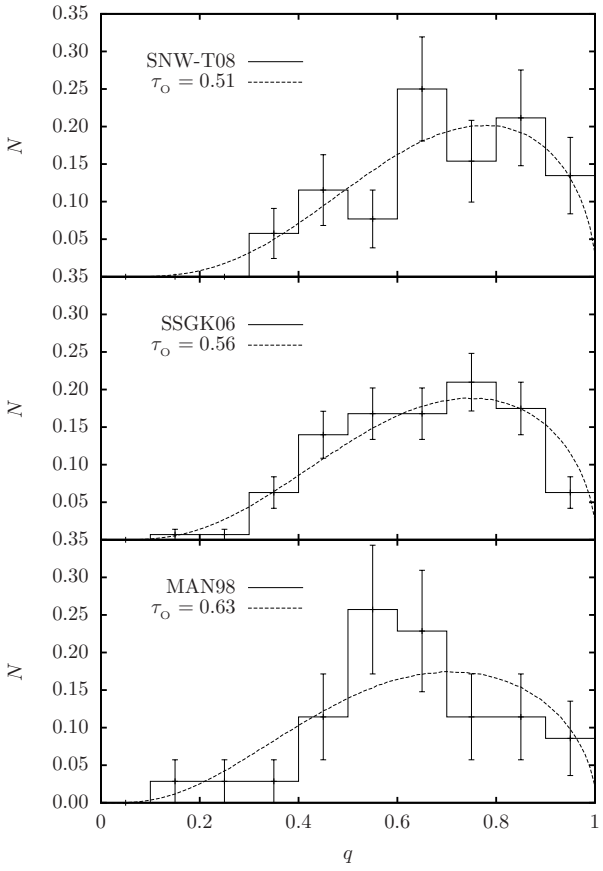

Figure 5. The histograms represent the distributions of aspect ratio obtained by SSGK06 (top), MAN98 (middle) and SNW-T08 (bottom), with $\sqrt{N}$ errors. The dashed lines represent the best fits obtained with **M1**.

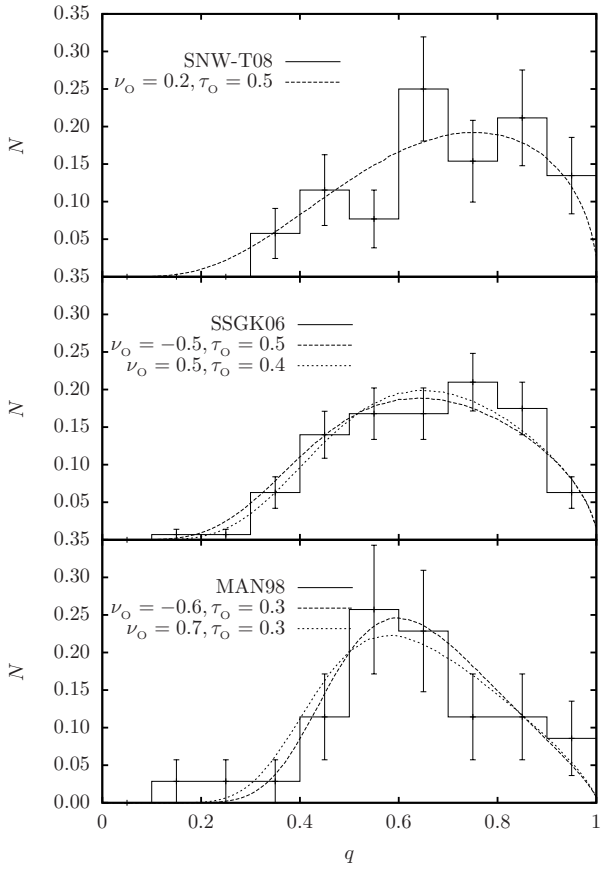

Figure 6. As Fig. 5, but for **M2a**.

4.5 Model selection

We quantify the quality of the different models, for the different data sets, by calculating Bayes factors, $K_{\mathbf{k}\mathbf{k}'}$, as described in Section 3.3. The results are presented in Table 1, where $K > 1$ indicates a preference for the model denoted in the column header, and $K < 1$ indicates a preference for the model in the row label. Jeffreys (1961) suggests the following qualitative interpretation for different values of $K_{\mathbf{k}\mathbf{k}'}$:

$$
\begin{aligned}
K_{\mathbf{k}\mathbf{k}'} \leq 1/10 &\quad \text{Strongly supports } \mathbf{M}_{\mathbf{k}'}\,,\\
1/10 < K_{\mathbf{k}\mathbf{k}'} \leq 1/3 &\quad \text{Moderately supports } \mathbf{M}_{\mathbf{k}'}\,,\\
1/3 < K_{\mathbf{k}\mathbf{k}'} < 1 &\quad \text{Weakly supports } \mathbf{M}_{\mathbf{k}'}\,,\\
K_{\mathbf{k}\mathbf{k}'} = 1 &\quad \text{No preference}\,,\\
1 < K_{\mathbf{k}\mathbf{k}'} < 3 &\quad \text{Weakly supports } \mathbf{M}_{\mathbf{k}}\,,\\
3 \leq K_{\mathbf{k}\mathbf{k}'} < 10 &\quad \text{Moderately supports } \mathbf{M}_{\mathbf{k}}\,,\\
K_{\mathbf{k}\mathbf{k}'} \geq 10 &\quad \text{Strongly supports } \mathbf{M}_{\mathbf{k}}\,;
\end{aligned}
$$

we stress that these categories are only intended to be indicative.

The SNW-T09 data are much better fitted by **M1** or **M2b**, than by **M2a** or **M4**; there is little to chose between **M1** and **M2b**. Conversely, the SSGK06 and MAN98 data sets are both fitted best by **M2a**, with **M1** also giving a good fit, and **M2b** and **M4** giving relatively poor fits. To combine the data sets, we have simply taken the products of their individual Bayes factors, and these are given in the last panel of Table 1. These values suggest that **M1** is the best model. **M2a** is almost as good, and should remain in the reckoning against the day when sufficient data is available to distinguish between filamentary and disc-like cores.

Since our analysis has not included the errors on individual data points (they are not available), the Poisson errors in Figs. 5 and 6, and in Eqn. (3.5), should be larger. This would broaden the posterior PDFs for all models, but the effect would tend to be larger for models with more free parameters, in the sense that the probability would be smeared over more dimensions, and therefore their marginal likelihoods would be reduced more. Since we have already concluded that **M1** performs best, we infer that this conclusion would be reinforced if observational errors were included.

5 CONCLUSIONS

We have used Bayesian analysis to infer the intrinsic shapes of prestellar cores in Ophiuchus. We find that the observational data is well fitted with a one-parameter model, **M1**,

SNW-T08				
	M1	**M2a**	**M2b**	**M4**
M1	1	0.31	1.02	0.08
M2a	3.20	1	3.27	0.26
M2b	0.98	0.31	1	0.08
M4	12.11	3.78	12.36	1
SSGK06				
	M1	**M2a**	**M2b**	**M4**
M1	1	1.80	0.31	0.48
M2a	0.56	1	0.17	0.27
M2b	3.23	5.80	1	1.54
M4	2.10	3.76	0.65	1
MAN98				
	M1	**M2a**	**M2b**	**M4**
M1	1	1.76	0.75	0.60
M2a	0.57	1	0.43	0.34
M2b	1.33	2.34	1	0.80
M4	1.67	2.93	1.25	1
COMBINED				
	M1	**M2a**	**M2b**	**M4**
M1	1	0.98	0.24	0.023
M2a	1.02	1	0.24	0.024
M2b	4.21	4.21	1	0.10
M4	42.5	41.6	10.0	1

Table 1. Bayes factors, $K = P(\mathbf{M}_{\rm COLUMN}|\mathbf{D})/P(\mathbf{M}_{\rm ROW}|\mathbf{D})$, calculated using Eqn. 3.10. The first three panels give values for the individual data sets, and the fourth panel gives their product.

in which cores are triaxial ellipsoids with axes chosen from a log-normal distribution having zero mean and standard deviation $\tau_{\rm O} \simeq 0.57 \pm 0.07$. The two-parameter models, **M2a** and **M2b**, do not sufficiently improve the fit to justify their adoption, and the four-parameter model, **M4** is completely unjustified.

REFERENCES

Binney J., 1985, MNRAS, 212, 767

Goodwin S. P., Ward-Thompson D., Whitworth A. P., 2002, MNRAS, 330, 769

Jeffreys H., 1961, The Theory of Probability. Clarendon Press, Oxford, third edition, p. 432

Jones C. E., Basu S., 2002, ApJ, 569, 280

Motte F., Andre P., Neri R., 1998, A&A, 336, 150

Myers P. C., Fuller G. A., Goodman A. A., Benson P. J., 1991, ApJ, 376, 561

Ryden B. S., 1996, ApJ, 471, 822

Simpson R. J., Nutter D., Ward-Thompson D., 2008, MNRAS, 391, 205

Stanke T., Smith M. D., Gredel R., Khanzadyan T., 2006, A&A, 447, 609

Stutzki J., Güsten R., 1990, ApJ, 356, 513

Tassis K., 2007, MNRAS, 379, L50

Weinberg M. D., , 2009, Computing the Bayesian Factor from a Markov chain Monte Carlo Simulation of the Posterior Distribution, arXiv:0911.1777